Passive seismic imaging of ore deposits using coda wave interferometry: a case study of Akanvaara V-Cr-PGE deposit in Northern Finland

Nikita Afonin[1], Elena Kozlovskaya[1], Kari Moisio[1], Shenghong Yang[1], Jouni Sarala[1]

[1]Oulu Mining School, University of Oulu, Oulu, 90570, Finland

Correspondence to: Nikita Afonin (nikita.afonin@oulu.fi)

Abstract. In this study, we present an innovative method to image the inner structure of orthomagmatic ore deposits using P-wave coda of regional seismic events. We combine data processing and interpretation schemes from conventional passive seismic interferometry and teleseismic receiver function (RF) method. We hypothesize that correlation of P-wave coda recorded by three-component sensors can be used to evaluate body wave part of empirical Green's tensor, from which arrivals of reflected and converted waves could be extracted. To test our hypothesis, we installed a high-resolution seismic array (profile) with 606 seismic instruments on the Akanvaara V-Cr-PGE deposit in Northern Finland above the inclined zones of V-Cr mineralization, placed inside ultramafic intrusion. From the regional seismic catalogue, provided by the Institute of Seismology, University of Helsinki, we selected the P-wave coda of 363 regional seismic events to evaluate body wave part of empirical Green's tensor by passive seismic interferometry. Further interpretation of the tensor allowed us to identify arrivals of PS and SP waves, converted at Cr and V mineralization zones. We conducted numerical simulation of plane wave interaction with the synthetic Akanvaara deposit model compiled from geological and drilling data and found that Green's tensors evaluated from synthetic seismograms and from seismic data contain similar converted PS and SP arrivals. To calculate depths to the conversion boundaries, we obtained S-wave velocity model using MASW method. According to calculated depths and geological model compiled from drilling data we suggest that the converted arrivals correspond to continuation of the Cr and V mineralized zones. Therefore, using the empirical Green's tensor, evaluated from P-wave coda of regional seismic events can be an effective tool for orthomagmatic ore deposits exploration in both greenfield and brownfield cases. In this paper we are describing details of the passive seismic experiment, numerical simulation, data processing and interpretation.

1 Introduction

Critical raw materials (CRM) are fundamental for a wide set of EU strategic sectors such as aerospace, digital industry, and defence sectors (European Commission, 2023a). Moreover, the EU green energy transition followed by an increase in the production of solar panels, wind turbines, electric vehicles and energy efficient lighting, where CRM such as platinum-group metals (PGM), nickel (Ni), cobalt (Co), vanadium (V), copper (Cu) are irreplaceable. Orthomagmatic mineral systems

30   include mafic layered intrusions and conduit type sulphide deposits, which host many of the above-mentioned CRMs. In the EU, there is currently only one orthomagmatic sulphide deposit (Kevitsa Ni-Cu-PGE-Co, Finland) and one orthomagmatic oxide deposit (Kemi Cr, Finland) in production. However, there are potential deposits in different countries, one of the important belts is the mafic layered intrusions in northern Finland, which host a number of mineralizations, such as PGE in Portimo, Penikat, V-Ti oxide in Koillismaa and Akanvaara, Chromitite in Kemi (Maier and Hanski, 2017).

35   This study is a part of the SEMACRET project ("Sustainable exploration for orthomagmatic (critical) raw materials in the EU: Charting the road to the green energy transition") where one of the goals is to develop environmentally friendly methods to explore inner structure of orthomagmatic ore deposits. One of the types of such deposits is mafic layered intrusion, where often the ore hosted in layers. Therefore, constraining the internal layering of these intrusions can provide critical information about ore layers.

40   Currently, the exploration industry uses extensive exploration drilling and drillcore data analysis to detect mineralized zones inside such intrusions. Application of non-invasive geophysical techniques, like controlled source seismics (CSS), is challenging, as mineralization is often confined to near-vertical relatively thin layers. Delineation of such boundaries by traditional ground-based controlled-source seismic profiling with one-component sensors is problematic because of absence of reflected arrivals from such boundaries on seismograms (Bohlen et al., 2003; Malehmir et al., 2012b). One of the ways to

45   investigate such boundaries by seismic methods is using vertical seismic profiling (VSP) (e.g. Greenhalgh et al., 2003), in which the waves converted at sub-vertical boundaries can be detected. Nevertheless, this is quite an expensive and not environmentally friendly method as its implementation requires drilling and usage of active seismic sources (usually blasts).

In this study we try to solve the problem using passive seismic methods, which are based on the recording and processing of ambient seismic noise (e.g. Afonin, 2022). Compared to CSS, the passive seismic methods are more environmentally

50   friendly, as they do not need to use artificial sources of seismic energy such as blasts or vibrotrucks.

Ambient noise seismic interferometry can be an effective tool to solve applied tasks in the case when strong enough ambient noise sources are existing around the studied area. For example, this method is effective in study area, like near industrial objects or urban areas, mines, roads etc. In remote and seismically quiet areas, this method requires special algorithms to improve the quality of empirical Green's functions (EGF) (e.g. Afonin et al., 2019). Nevertheless, results of case studies

55   done in remote and quiet areas of Northern Finland demonstrated that this technique only allows retrieving the surface wave part of EGF (Afonin et al., 2021).

During the past decade, several passive seismic methods not related to ambient noise analysis have been developed. Usually, such methods use records of teleseismic earthquakes. The most popular among these methods are receiver function method originally proposed by Vinnik (1977), teleseismic coda wave interferometry (e.g. Sneider, 2006) and autocorrelation of

60   teleseismic P-wave coda (e.g. Wang et al., 2020). These methods have been used to study the deep structure of the Earth's crust and upper mantle because of the low frequency content of the used signal (up to several Hz). However, such frequencies are too low for the detection of near surface objects like in the ore exploration which would require frequencies comparable to those used in CSS experiments (dozens of Hz).

In this study we utilised the theoretical background and principles of receiver function method, passive seismic
65   interferometry, and controlled source seismic exploration to apply passive seismic methods for exploration tasks.
Considering the theory of seismic wave propagation in layered medium (Aki and Richards, 2002) and that mineralization
zones inside the Akanvaara layered intrusion are presented as inclined thin layers, we assumed that P-wave coda, recorded
above such mineralization zones should include PS and SP waves converted on these thin layers. These converted arrivals
should be visible in non-diagonal empirical Green's tensor components.
70   In the next chapters we present the description of the developed method, details of passive seismic experiment together with
the geological background of the area and results of the data processing, numerical simulation and interpretation.

2 Geological characteristics of the studied area and passive seismic experiment description

The Kenorland supercontinent is composed of several Archaean cratons including Karelian, Kola in Fennoscandia, Superior
in Canada, and Woyming in the USA. Starting from early Proterozoic (2.5 Ga), the supercontinent starts to rift. Multiple
75   generations of mafic-ultramafic magmatism finally break the continent at about 2 Ga ago with the formation of oceanic
crust. The early-stage magmatism, dated at 2.44 - 2.5 Ga, consists of a dozen of mafic layered intrusions, numerous mafic
dyke swarms, mafic-ultramafic volcanic rocks in rifting belts, as well as minor amount of felsic igneous rocks (Lauri et al.,
2006). The mafic layered intrusions occur mainly at the boundary between Archaen granite-gneiss basement and overlying
Paleoproterozoic supracrustal belt, and host different types of mineralization (Maier and Hanski, 2017). Many 2.45 Ga
80   intrusions belong to the Tornio-Näränkävaara intrusion belt running from the western to the eastern border of Finland (e.g.,
Kemi, Koillismaa), and the Akanvaara and Koitelainen intrusions are located in Central Lapland Belt (CLB) in northern
Finland (Fig. 1, a).
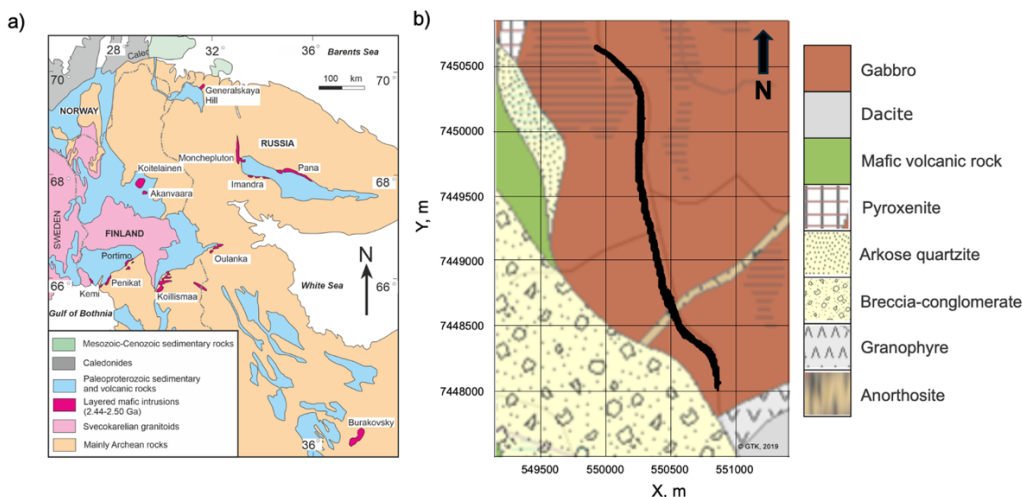
Figure 1: Studied area: a) Geological map showing mafic layered intrusions in the Fennoscandian Shield, modified after Alapieti et
85   **al., 1990, and Pripachkin et al., 2013; b) Akanvaara seismic profile on the bedrock map (coordinate system is ETRS 1989**
TM35FIN NE. X axis means East direction, Y axis means North direction).

The CLB includes Archaean basement rocks (2830-2680 Ma) consisting of mainly granodioritic and tonalitic igneous complexes, granitic gneisses and minor greenstone belts (Koistinen et al., 2001, Hanski et al., 2001; Konnunaho et al., 2013;

90 Moilanen et al., 2019). The Archaean basement of the area is covered by Paleoproterozoic supracrustal lithology including multiple generations of volcanic formations from 2.5 to 1.98 Ga. The oldest volcanic formation (2.5-2.44 Ga) is co-genetic with the 2.5-2.44 Ga mafic layered intrusions, with composition varying from ultramafic to felsic metavolcanic rocks.

The Akanvaara intrusion is a block-faulted mafic layered intrusion with monoclinic structure dipping to SE at angles of 25–40°. The rocks of the intrusion and country rocks have undergone amphibolite facies regional metamorphism, resulting in

95 variable degrees of hydration and recrystallization of cumulates (Mutanen, 1998).

The Akaanvaara intrusion was extensively studied by the Geological Survey of Finland (GTK) during the 1990's, when more than 100 diamond drill holes were drilled with comprehensive geochemical analyses across the whole stratigraphy. The 3.1 km thick layered rocks are subdivided into Lower, Middle and Upper Zones, with thicknesses of approximately 640, 570 and 1900 m, respectively (Mutanen, 1997; Hanski et al., 2001). The Lower Zone (LZ) is mainly composed of pyroxenite

100 with minor olivine bearing rocks, and the Middle Zone (MZ) is containing noritic rocks and anorthosite, and towards gabbroic rocks and ferrogabbros in the Upper Zone (UZ). According to these results and magnetic survey (Mutanen, 2005), at least 23 chromitite layers have been identified from Lower Zone to Middle Zone with thickness from several centimetres to several meters. Multiple layers with elevated PGE contents occur in the LZ and MZ with very minor amount of sulphide. One important potential resource is the magnetite gabbro occurring in the UZ with a thickness of several hundred meters.

105 The mineralized zones have lengths of approximately 6.5 km along strike (Fig. 2, a).
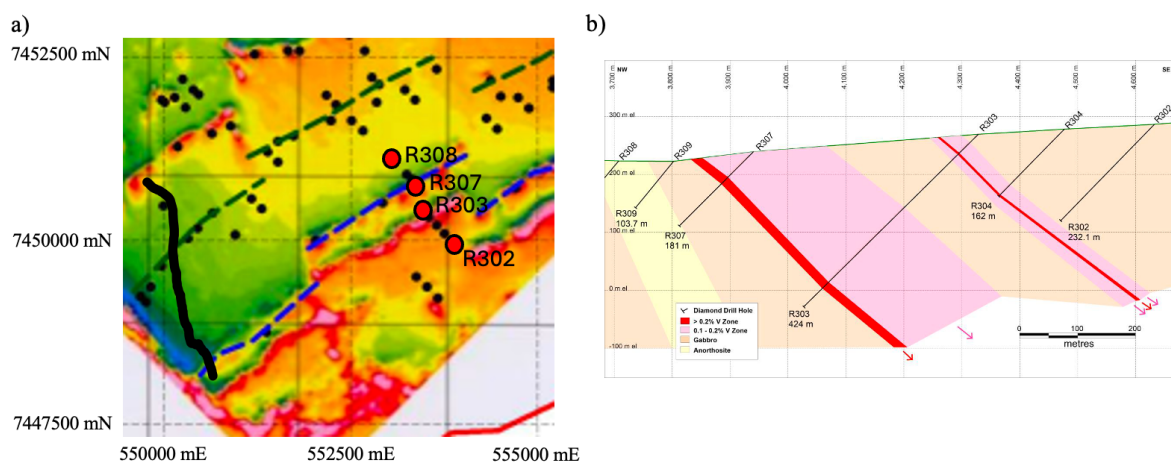
Figure 2: (a) Drilling, Mineralized Targets, Total Magnetic Field (adopted with modifications from Lutynski, 2019): green dashed line – upper chromite vanadium target; blue dashed line – magnetite gabbro vanadium target; red and black circles – drill holes; black curve – passive seismic profile. (b) lithological cross-section compiled from drilling data (Lutynski, 2019). Magnetic data
110 **from Geological Survey of Finland.**

The well layered rocks and occurrence of thick magnetite gabbro motivated selection of Akanvaara as one of the sites in SEMACRET project for testing of advanced geophysical techniques for orthomagmatic mineral deposits exploration.

For testing the passive seismic interferometry technique, we decided to acquire the data along a high-resolution passive seismic profile with total length of 3 km crossing several mineralization zones of Cr and V in the Akanvaara intrusion (Fig. 2, a). In the experiment total of 606 GSB-3 seismic recorders with 5 Hz three-component seismic sensors manufactured by Geospace Technologies Ltd. (USA) were used. Devices were provided by the Finnish FLEX-EPOS seismic instrument pool. We installed these instruments alongside a road, with a 5 m spacing between sensors (Fig. 1, b). The in-line component of sensors was oriented to NS direction and devices recorded continuous seismic data from 2.11.2023 to 9.12.2023 with a sampling frequency of 500 Hz.

We used the online seismic bulletin by the Institute of Seismology of the University of Helsinki (https://www.helsinki.fi/en/institute-seismology) to compile a list of 363 seismic events (both earthquakes and production blasts) that occurred during the registration period from epicentral distances between 250 – 800 km. Previous results of wide-angle reflection and refraction profiles in northern Finland and modelling of propagation of body waves in the crust (Tiira et al., 2014; Janik et al., 2009) demonstrated that the first arrivals of body waves of local and regional seismic events recorded at such distances are the Pn and Sn phases that are refracting in the uppermost mantle beneath the Moho boundary and arrive at sub-vertical incidence to seismic stations in the case of epicentral distances exceeding 250 km. In this case the coda of Pn and Sn would contain the secondary arrivals of P-and S-waves, including the waves converted at intracrustal boundaries with high acoustic impedance contrast. As the wavelengths of Pn and Sn waves are hundreds of meters and their incidence angles are sub-vertical, it is possible to consider them as plane waves for seismic arrays with distance between sensors smaller than the wavelengths. This knowledge justifies application of similar principles of converted waves detection by stacking of recordings of multiple events located at different azimuths, as proposed in receiver function (RF) techniques, (Vinnik, 1997) and utilize similar interpretation techniques.

The selected seismic events are mainly production blasts in quarries of Kola peninsula and Sweden and their locations are shown in Fig. 3.
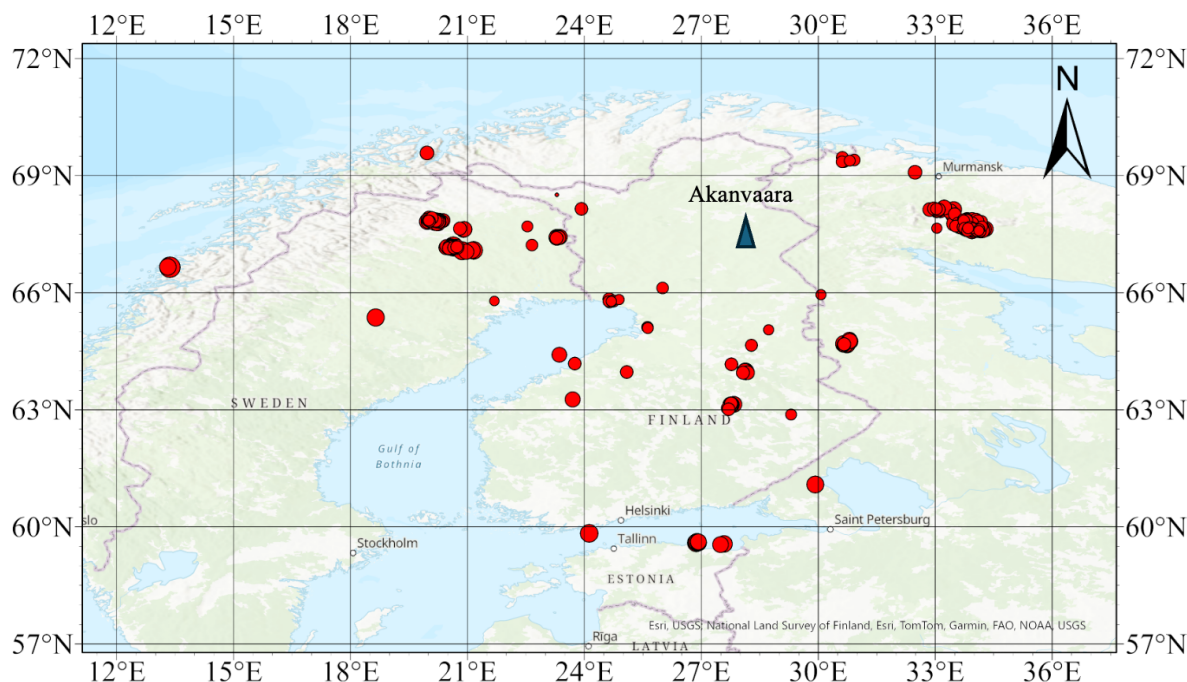
Figure 3: Sources of the seismic events, used in the study.

Also, several natural local earthquakes of relatively high magnitudes were recorded during the experiment. An example of
140   seismograms of such an earthquake is presented in Fig. 4. On these seismograms clear Pn and Sn arrivals are seen, as well as some scattered arrivals in their coda, which could be converted waves. Although, Sn coda can be used to evaluate empirical Green's tensor, we used only Pn coda in our study (blue dashed rectangle in Fig. 4) to avoid possible issues in interpretation caused by superposition of different waves.

To select frequency band for prefiltering coda before correlation, we calculated spectra of all the selected coda signals. To
145   exclude all possible local effects which can distort the results of spectral analysis (local small-scale heterogeneities, random noise, transport, etc.), we averaged spectra for each selected event over seismograms recorded by all seismometers. The sequence of these spectra is presented in Fig. 5.
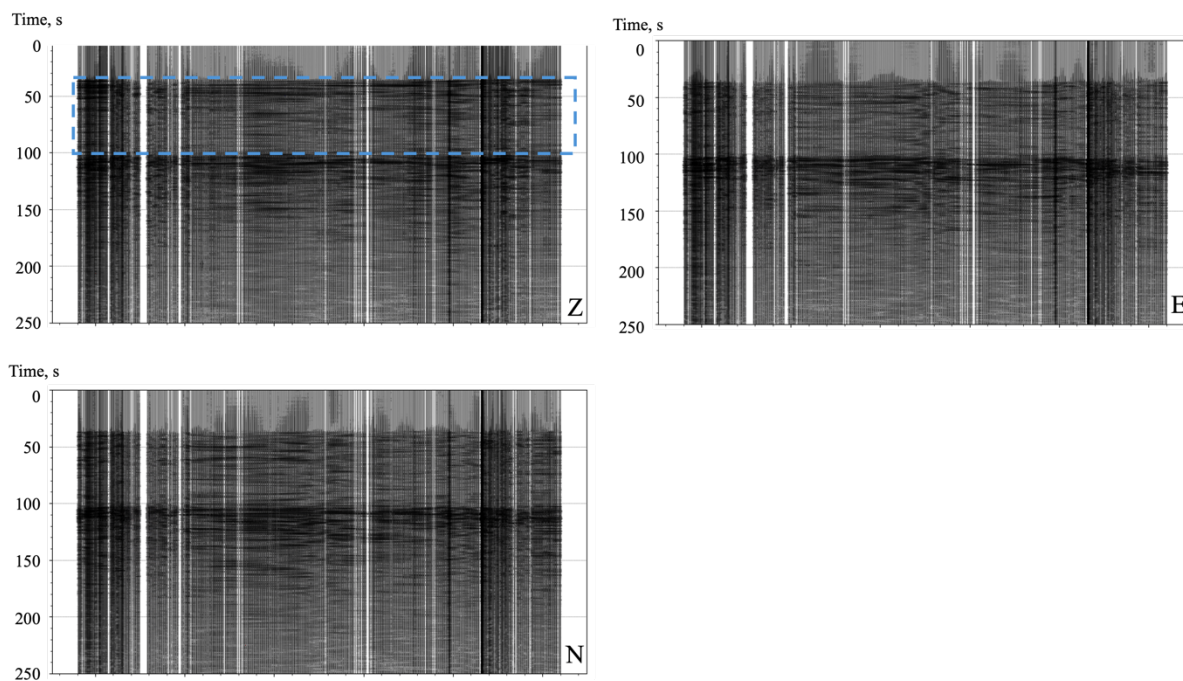
Figure 4: Seismograms of seismic event originated on 8.11.2023 (latitude=66.652, longitude=13.373 Ml=3.1 (Institute of seismology, University of Helsinki)) and recorded by the profile. P-wave coda contoured by blue dashed rectangle.
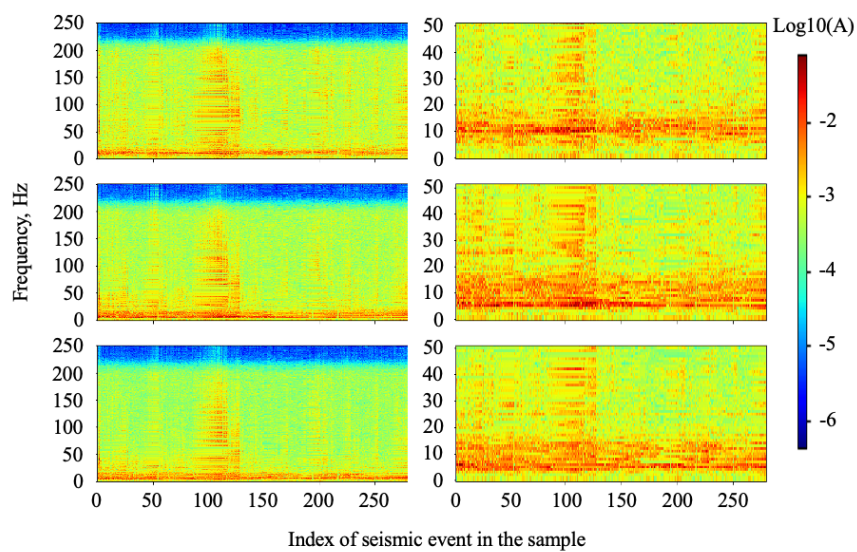
Figure 5: Frequency content of P-wave coda of selected seismic events.

155 All selected P-wave codas have high amplitudes in the frequency range of about 5-15 Hz. In spite that amplitude normalization was not applied, it is evident that some of the P-wave codas also have high-frequency content in wide range from 5 to about 200 Hz (seismic events with indexes from about 100 to approximately 120 in Fig. 5). High frequency signals can potentially be used for studying the shallow subsurface: from the ground surface down to several dozens of meters. However, we selected a frequency band of 10-15 Hz for our study, as signal with such frequency is better for our target

160 depths of investigation – from several dozen meters to several kilometres.

3 Method

3.1 Theoretical background

Methods, based on correlation or deconvolution transforms of seismic records aiming to study deep crustal structure are already well established for some time. The method for retrieval of reflected response from transmission response for the

165 medium beneath seismic sensor by autocorrelation has been introduced by Clearbout (1968). Obtaining radial receiver function from teleseismic P-wave coda by deconvolution of vertical seismograms from horizontal have been presented by Vinnik (1977). Wang et al., (2020) successfully used autocorrelation functions of teleseismic P-wave coda to obtain reflections from boundaries in the Earth's crust.

To study near surface using P-wave coda of regional seismic events, we involved interferometric redatuming principles,

170 described in Shuster (2009), namely vertical seismic profile to surface seismic profile correlation transform (VSP to SSP) and modified this for case of converted waves (Fig. 6).
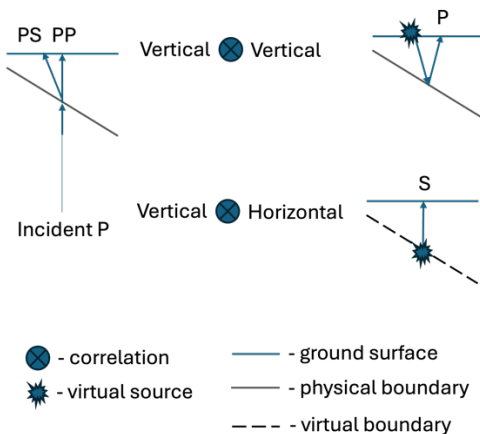
Figure 6: Interaction of plane wave with inclined boundary and interferometric redatuming (Shuster, 2009)

175 If the P-wave is converted to S-wave at a boundary with high acoustic impedance contrast and the incidence angle is large, then the amplitude of a PS wave can be of significant part of the P-wave amplitude (Aki and Richards, 2002). In this case correlation function of a vertical component of P-wave coda with horizontal ones should include converted arrivals.

Nevertheless, in this case we cannot use interferometric redatuming in its original form, because we deal with converted arrivals and therefore, we should consider virtual source on co-called virtual boundary inside the medium (Fig. 6). To calculate depth to the physical boundary, where converted wave originated, one can use the formula (Zhu and Kanamori, 2000):

$$H = \frac{t_{ps}}{\sqrt{\frac{1}{V_s^2} - p^2} - \sqrt{\frac{1}{V_p^2} - p^2}}, \tag{1}$$

where p is the ray parameter of the incidence P-wave; t_{ps} is time lag between direct P and converted PS waves; V_P and V_S are P- and S- velocities above a conversion boundary.

In the case when epicentral distances of seismic events are large compared to the size of a recording array and taking into account normalization that results from correlation procedure (Bostock, 2004), we can neglect the ray parameter and assume it equal to zero. Therefore Eq. (1) can be simplified:

$$H = (V_P - V_S)t_{ps}. \tag{2}$$

In that case t_{ps} is a time lag on correlation function that corresponds to converted PS or SP arrivals. In the case of strong acoustic impedance contrast, these arrivals should be clear visible on correlation functions, calculated between vertical and horizontal components of P-wave coda. To test this approach with synthetic data, we conducted numerical simulation of propagating plane wave through the model having similar geometry and elastic properties (seismic velocities and densities) as in the Akanvaara intrusion with imbedded mineralized layers.

3.2 Numerical simulation of P-wave coda scattering on inclined layers

The model (Fig. 7) used in the simulation represents a package of inclined layers composed of the major lithologies revealed in the Akanvaara intrusion by drilling (Table 1). Such features of mineralized zones inside the intrusion as their number, thicknesses of each zone, dip angle (Fig. 2), elastic properties and densities of layers material, were taken from existing geological and petrophysical information (Lutynski, 2019; Schön, 2015; Dortman, 1992). As incidence waves, we considered both P and S plane waves, arriving vertically from the model's bottom to its surface. According to the results of spectral analysis of P-wave coda in our field experiment (Fig. 5), we select the frequency equal to 10 Hz was used for these waves. To retrieve synthetic seismograms, we placed 300 receivers with an interval of 10 m on the top of the model, i.e., ground surface.

We simulated 5 different cases, with different values of mechanical properties between layers and host medium inside the intrusion (Table 1). We selected values for these properties which are typical for correspondent rocks of the Fennoscandian shield (Dortman, 1992; Schön, 2015). In Table 1 'Tasks' correspond to different mechanical properties of layers, while 'Subtasks' correspond to different source type (either P or S) of the plane wave.
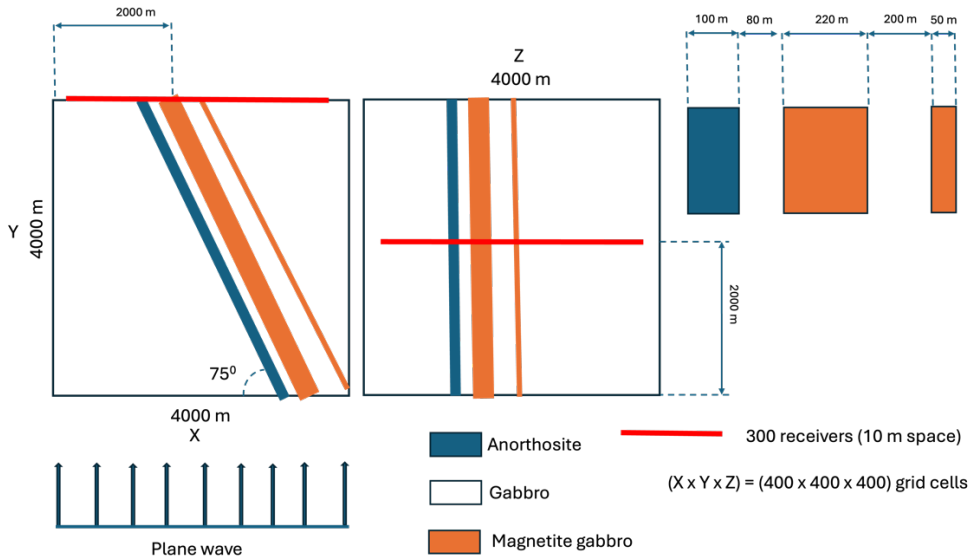
Figure 7: Synthetic model of Akanvaara deposit used in the numerical simulation. Y is depth.

210

Table 1 – Tasks description in the numerical simulation

Task	Sub task	Source type	Mechanical properties of layers								
			Anorthosite			Gabbro			Magnetite gabbro		
			Vp, m/s	Vs, m/s	Rho, kg/m³	Vp, m/s	Vs, m/s	Rho, kg/m³	Vp, m/s	Vs, m/s	Rho, kg/m³
1	1.1	P	6100	3450	2680	6450	3550	2950	6750	3175	2980
	1.2	S									
2	2.1	P	5500	3400	2630	6800	4100	3050	6100	2700	2970
	2.2	S									
3	3.1	P	5500	3400	2630	6800	4100	3050	7400	3650	2990
	3.2	S									
4	4.1	P	6700	3500	2730	6800	4100	3050	6100	2700	2970
	4.2	S									
5	5.1	P	6700	3500	2730	6800	4100	3050	7400	3650	2990
	5.2	S									

To demonstrate that the converted waves from the inclined layers can be observed even in the cases of low impedance contrast, we describe below the results of simulation, related to Task 1 (Table 1) for both source types, assuming that the P-wave coda of seismic event is presented by superposition of P- plane waves and S- plane waves of different polarizations.

215

To calculate synthetic seismograms, we used SOFI3D software (Bohlen, 2002) installed in Puhti cluster of Centre of Scientific computing of Finland. The simulation had run for a 400x400x400 grid corresponding to 4000 m in horizontal directions and 4100 m in vertical direction. The model had a 102.5 m thick layer of atmosphere on the top of the bedrock and the seismic sensors were placed on the boundary of the atmosphere and uppermost bedrock layer. The seismic source was set

220   to be at a depth of 3850m from the surface. The seismic source is simulated by exciting a force from every grid point in the layer at the excitation depth. A perfectly matched layer (PML) boundary condition layer of 150 m was applied on the sides and the bottom of the model, with a free surface boundary condition on top of the model. The simulation corresponds to 5.0 seconds of measurement with a sampling period of 0.0005 s. The models of the medium, as well as the homogeneous reference medium, were done with Matlab scripts. We calculated synthetic seismograms for a homogeneous medium, where

225   elastic properties correspond to those of the host rock, as well as for the model with inclined layers (Fig.7).

To improve visibility of scattered arrivals and for further comparison with correlation functions, we subtracted these synthetic seismograms from each other. Fig. 8 shows synthetic seismograms, calculated for the P-plane wave.
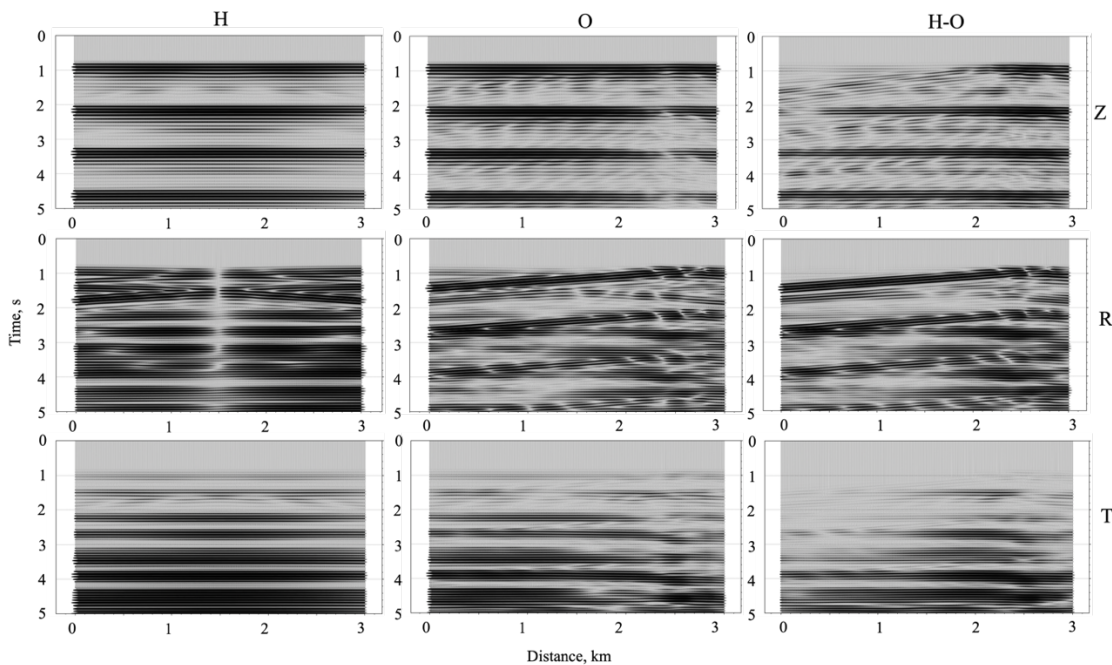
Figure 8: An example of synthetic seismograms, which correspond to task 1.1 (Table 1). H column – synthetic seismograms for
230   **case of homogeneous medium (gabbro); O column - synthetic seismograms for case of layered medium (Fig. 7); H-O – synthetic seismograms, obtained by subtraction of seismograms for layered medium from seismograms for homogeneous medium; Z, R, T – seismograms for horizontal, radial, and transverse channels.**

Next, we calculated correlation functions between all possible pairs of channels of synthetic seismograms to obtain synthetic

235   empirical Green's tensor (Fig. 9). On the ZR tensor's component clear PS converted arrivals are seen. Using the P- and S-

wave velocities of the host medium (Table 1) and the Eq. (2) it is possible to verify by calculating the depth to the boundary that these arrivals originate from layers which correspond to inclined zones with different lithology.
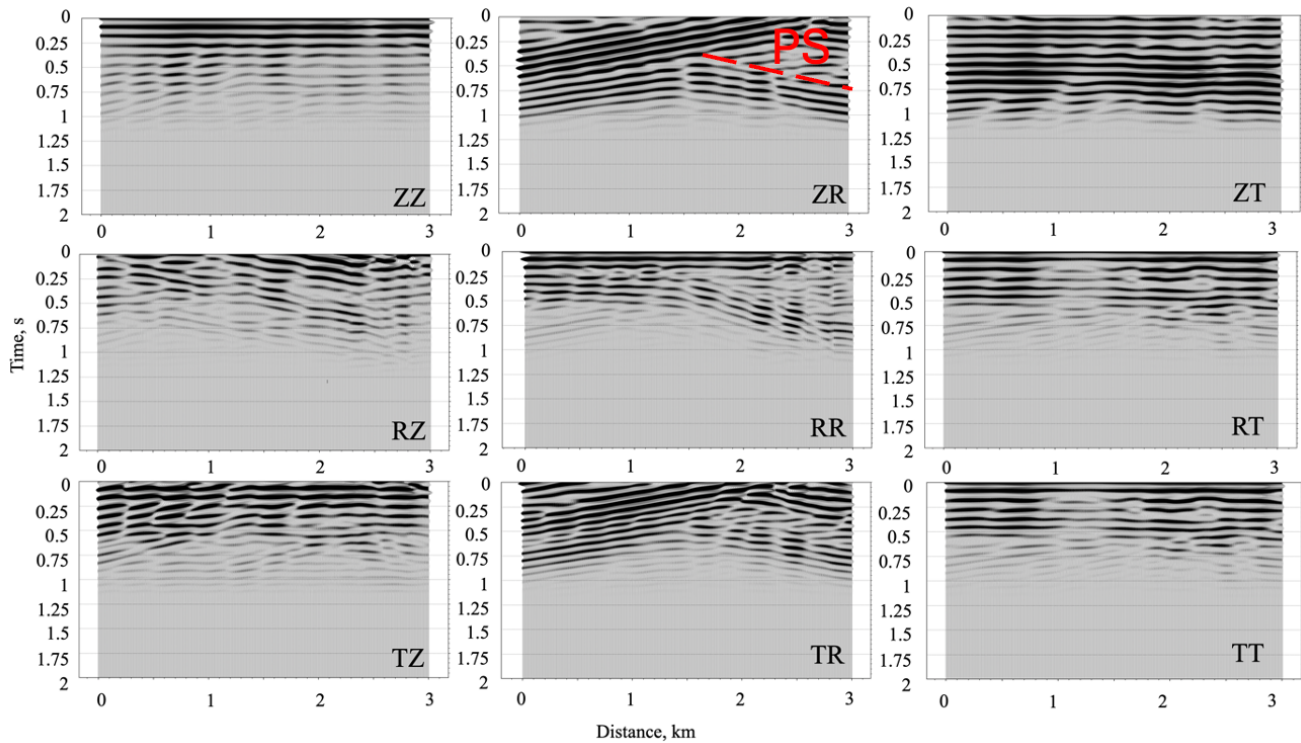
Figure 9: Correlation functions (causal parts), calculated for case of plane wave P as a source for corresponded pairs of synthetic
240 **seismograms channels, presented on Figure 8 (O-column).**

To analyse scattering of the plane S-wave the same procedure, as described above was done. We obtained synthetic seismograms for both cases: S-wave polarized along the line of seismometers (S-wave of radial polarization) and S-wave polarized perpendicular to the line of seismometers (S-wave of transverse polarization). Synthetic seismograms and
245 correspondent correlation functions are shown on Figures 10, 11, 12 and 13.
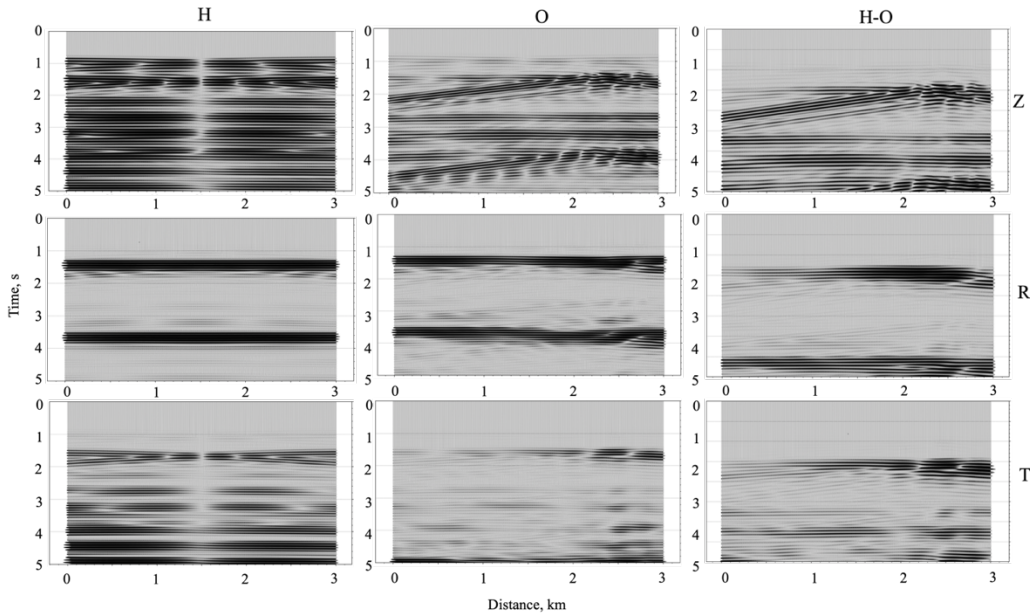
Figure 10: An example of synthetic seismograms, which correspond to task 1.2 (Table 1). H column – synthetic seismograms for case of homogeneous medium (gabbro); O column - synthetic seismograms for case of medium with intrusion (Fig. 7); H-O – synthetic seismograms, obtained by subtraction of seismograms for medium with intrusion from seismograms for homogeneous medium; Z, R, T – seismograms for horizontal, radial, and transverse channels.
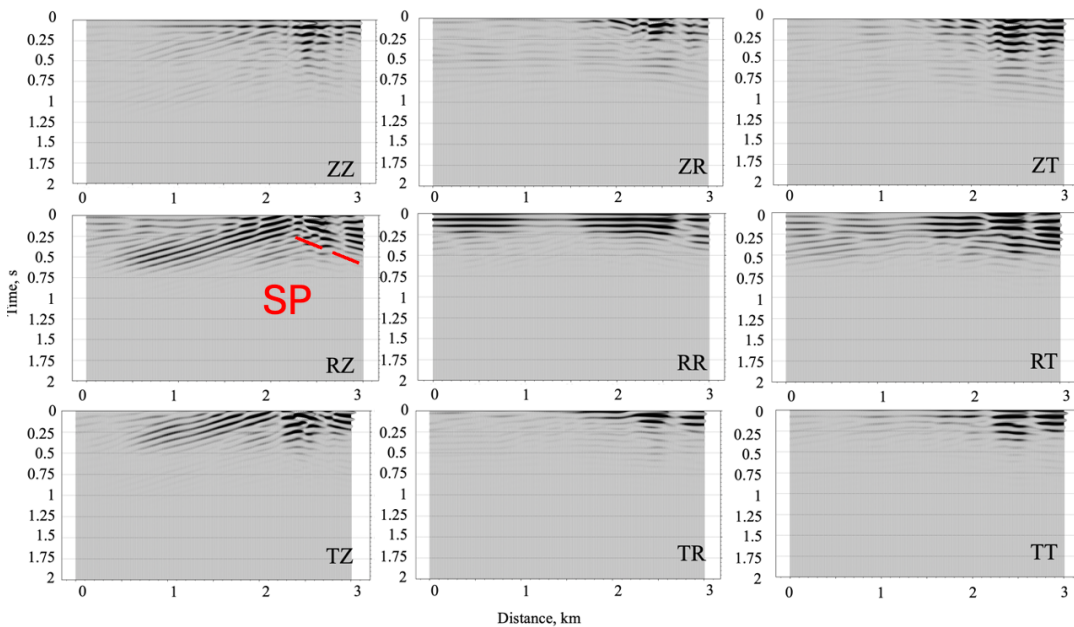
Figure 11: Correlation functions (causal parts), calculated for case of plane wave S (of R-polarization) as a source for corresponded pairs of synthetic seismograms channels, presented on Figure 10 (O-column).
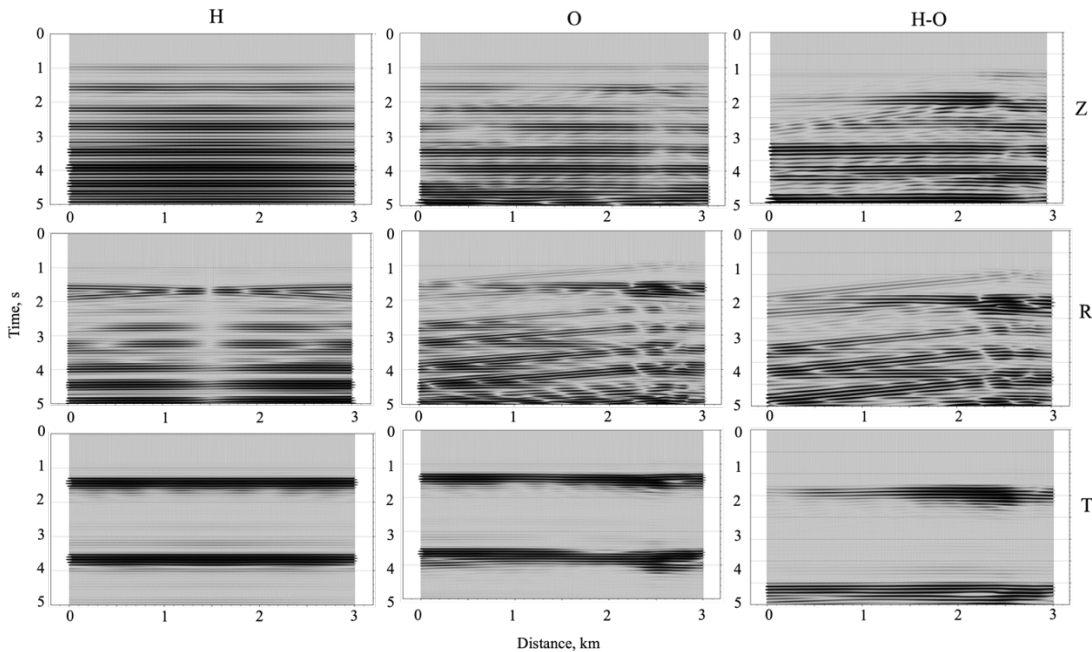
Figure 12: An example of synthetic seismograms, which correspond to task 3.1 (Table 1). H column – synthetic seismograms for case of homogeneous medium (gabbro); O column - synthetic seismograms for case of medium with intrusion (Fig. 5); H-O – synthetic seismograms, obtained by subtraction of seismograms for medium with intrusion from seismograms for homogeneous medium; Z, R, T – seismograms for horizontal, radial, and transverse channels.
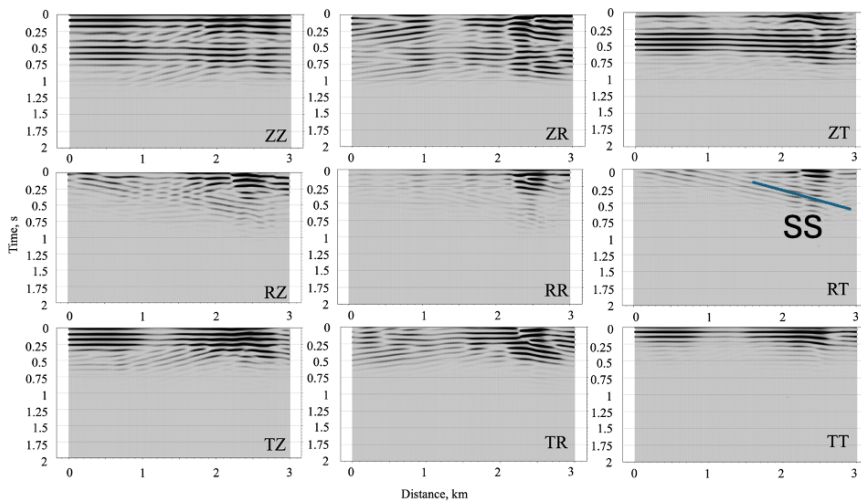
Figure 13: Correlation functions (causal parts), calculated for case of plane wave S (of T-polarization) as a source for corresponded pairs of synthetic seismograms channels, presented on Figure 12 (O-column).

The SP converted arrivals are clearly visible on RZ components of empirical Green's tensor (Fig. 11). Arrivals on the RT
270   tensor components (Fig. 13) can be interpreted as trapped S-waves (e.g. Bohlen, 2003).

4 Data processing

To obtain empirical Green's tensor from seismograms we applied prefiltering by bandpass filter of 10-15 Hz and one-bit
normalization (Bensen et al., 2007) preprocessing to P-wave coda. The one-bit normalization is necessary in our case
because it helps to improve visibility of converted arrivals on tensor components, as they have lower amplitudes comparing
275   to direct arrivals (Aki and Richards, 2002). Therefore, we need to use only phases of the signal and exclude analysis of
amplitudes from data processing. After preprocessing, we calculated correlation functions for all possible pairs of channels
for all stations of the array. For each station we stacked the calculated correlation functions over all seismic events to obtain
the body wave parts of empirical Green's tensors for each station. Causal parts of these tensors are presented as record
sections in Fig. 14, in which each trace corresponds to Green's tensor component for the particular station.
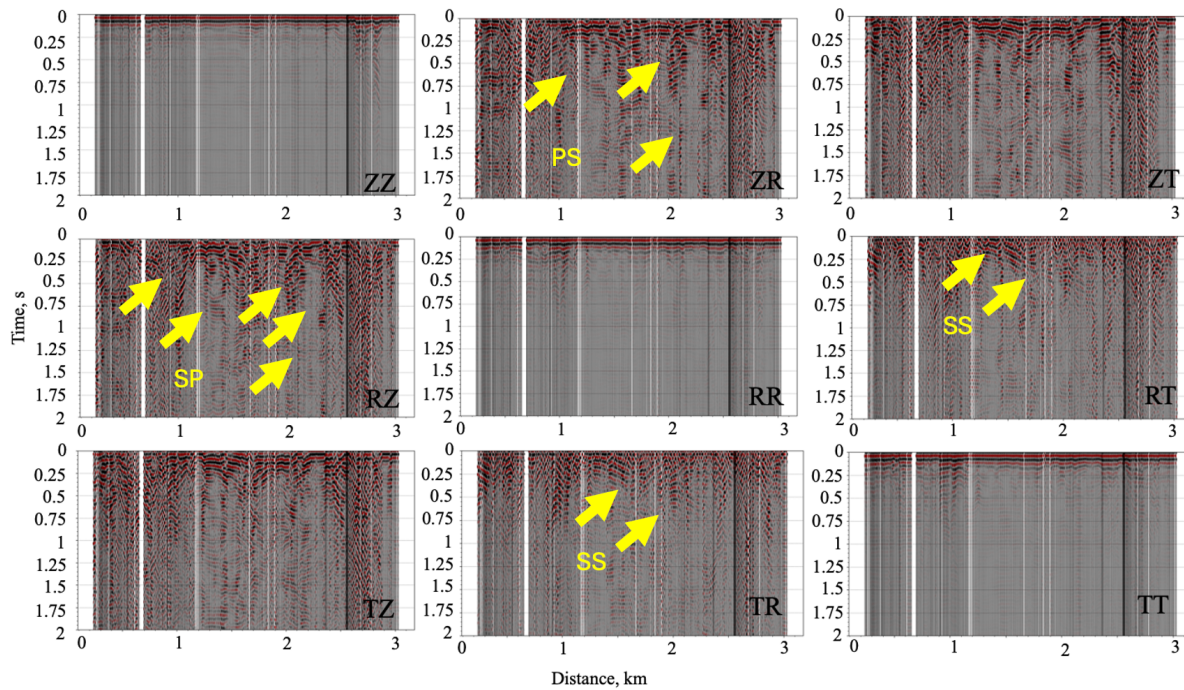
280

**Figure 14: Body-wave part of the empirical Green's tensor (causal parts) on frequency band of 10-15 Hz, evaluated by
autocorrelation of P-wave coda. Yellow arrows point to converted arrivals.**

In record sections of non-diagonal components of the tensors, one can see converted arrivals between offsets of about 0.5
285   and 2.5 km, namely, PS arrivals on ZR components, SP arrivals on RZ components and SS arrivals on RT and TR
components. Arrival times of these waves are increasing with offset, which indicates that they originated on an inclined

boundary. The PS and SP arrivals are also seen at time lags of about 0.15-0.25 s (ZR, ZT, RZ, TZ components). Because the time lags are near the same along the line, these waves originated on some horizontal boundary.

We compared these empirical Green's tenors with the synthetic Green's tensors presented on Figures 9, 11 and 13 and found quite a good similarity between them (Fig. 15), with exception of arrivals from the possible horizontal boundary. However, no horizontal boundary was included into our synthetic model.
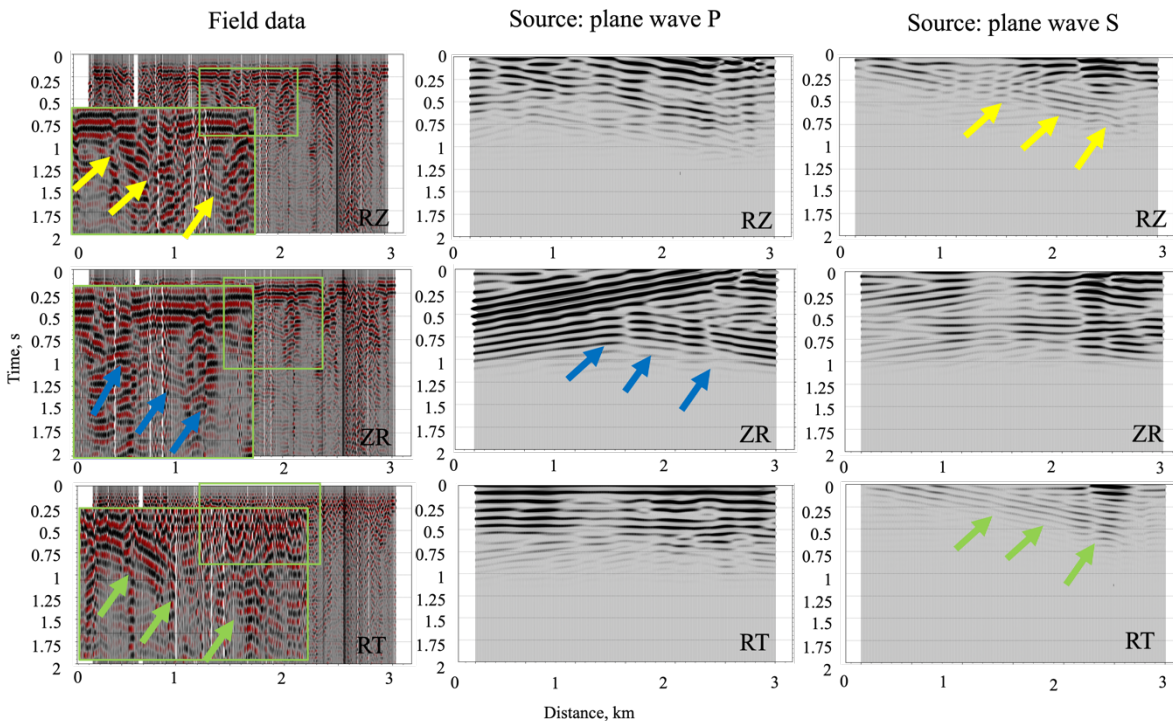
Figure 15: Non-diagonal empirical Green's tensors components and corresponding autocorrelation functions of synthetic seismograms: yellow arrows – SP converted arrivals; blue arrows – PS converted arrivals; trapped S-wave; green rectangles – zoomed parts of empirical Green's tensors components.

To calculate the depths to the conversion boundaries using Eq. (2), also information about P and S-waves velocities above these boundaries is needed. To get this information and to obtain the averaged velocity model below our seismic profile, we analysed surface waves of 37 seismic events located in-line with our profile to minimise the azimuthal effects. We selected surface wave parts of these events and pre-processed them with prefiltering by bandpass filter of 2-20 Hz and one-bit normalization. After this, we calculated cross-correlation functions of the vertical components of the seismograms between the seismogram corresponding to the virtual source position and all other seismograms recorded along the profile. We calculated frequency-velocity spectra of obtained cross-correlation functions using MASW technique (Park et al., 1999) with further extraction of dispersion curve in the frequency band of 3-6 Hz (Fig. 16).
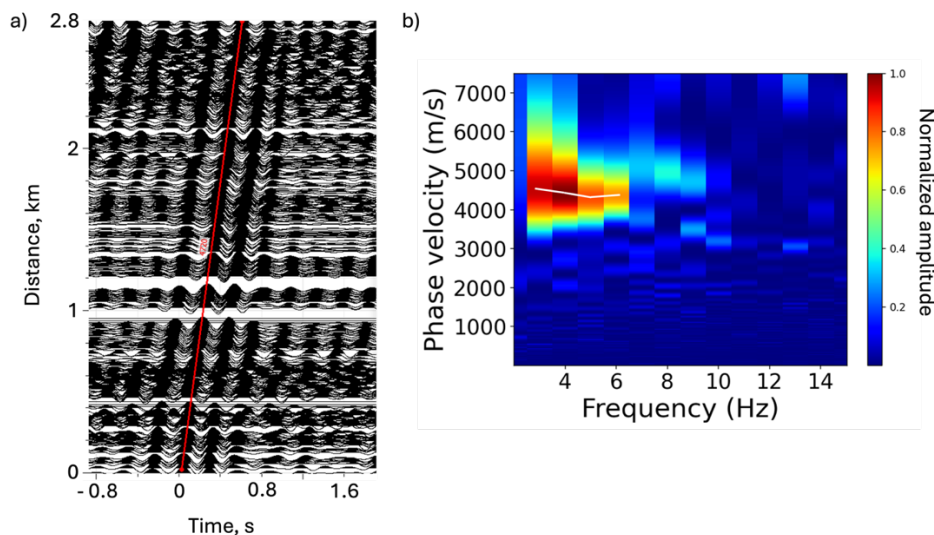
Figure 16: Surface wave part of empirical Green's functions on frequency band of 2-15 Hz (a) and correspondent dispersion curve (b).

310   The dispersion curves for higher frequency were not obtained with MASW because strong scattering of high frequency waves on the near surface heterogeneities makes it difficult to extract dispersion curves from frequency-velocity spectra. For near-surface velocities, we split the profile into several parts with lengths of about 500 m (Fig. 17) and calculated dispersion curves for these parts separately in the frequency range of 10-20 Hz using a set of narrow bandpass filters.
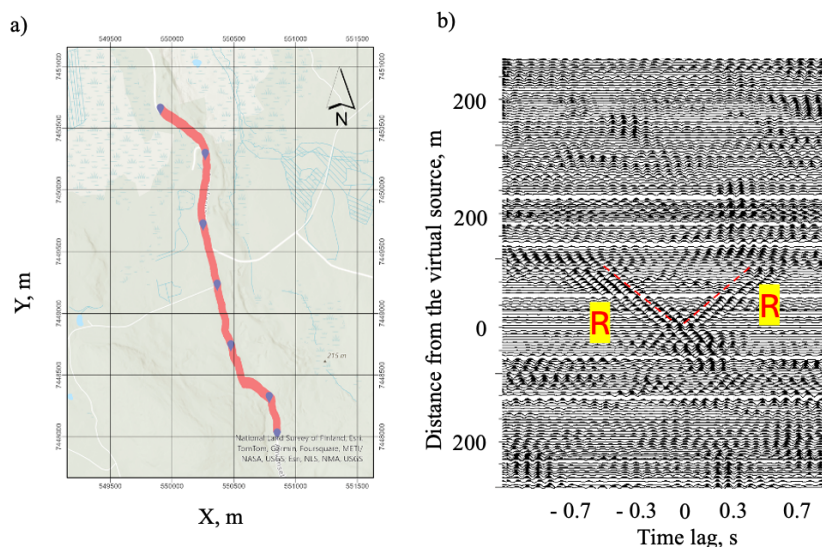
315   **Figure 17: Dispersion curve extraction on high frequency range: a) locations of "virtual sources" (©National Land Survey of Finland, Esri, TomTom, Garmin, Foursquare, METI/NASA, USGS; Esri, NLS, NMA,USGS); b) an example of cross-correlation functions, filtered by bandpass filter of 17-18 Hz and correspondent Rayleigh surface waves (R).**

In Fig. 17b an example of cross-correlation functions, filtered by bandpass filter of 17-18 Hz is shown. The arrivals of
320   surface waves are traceable at distances of 150-250 m from the virtual source. On the same figure are also arrivals which are
not related to direct surface waves but have significantly high amplitudes. These arrivals probably originate from near-
surface heterogeneities, and they are the main reason why obtaining dispersion curves using MASW is not possible in this
case.

As a result, we obtained one dispersion curve for low-frequency range, with the high S-wave velocities that may correspond
325   to the mafic- and ultramafic rocks of the Akanvaara intrusion, and four dispersion curves for high frequencies, with low
velocities that may correspond to quaternary sediments and/or fractured volcanic rocks near the surface. We could not
extract high-frequency dispersion curves for two parts of the profile, as clear surface wave arrivals are not visible on
correspondent cross-correlation functions.

We used the Monte-Carlo global optimization algorithm implemented in Geopsy software (www.geopsy.org) for dispersion
330   curves inversion. The ranges of model parameters for inversion are presented in Table 2. We used totally 500 iterations,
where on each iteration 2500 random models with properties from ranges in Table 2 were generated. For each of these
models, the theoretical dispersion curve was calculated and compared to that evaluated from cross-correlation functions of
surface waves. The solution of the inverse problem is the model with dispersion curve that fit the empirical one with the
minimum misfit.

335

Table 2 – Ranges of model parameters for inversion

Depth range, m	Vp range, m/s	Vs range, m/s	Density range, kg/m^3
1-30	200-850	100-500	1700-2650
5-35	200-1400	100-800	2600-2900
10-60	800-6000	500-3500	2700-3100
150-500	3700-7000	2700-5000	3000-3400

An example of the dispersion curve inversion result is presented on Fig. 18. The colour scale shows the misfit value between
theoretical and empirical dispersion curves, while black dots and lines are empirical dispersion curves. White colour
340   corresponds to the theoretical dispersion curve that matches the empirical one with the minimal misfit. Therefore, the white
colour on the velocity model plot shows the average 1-D S-wave velocity model for the studied medium.
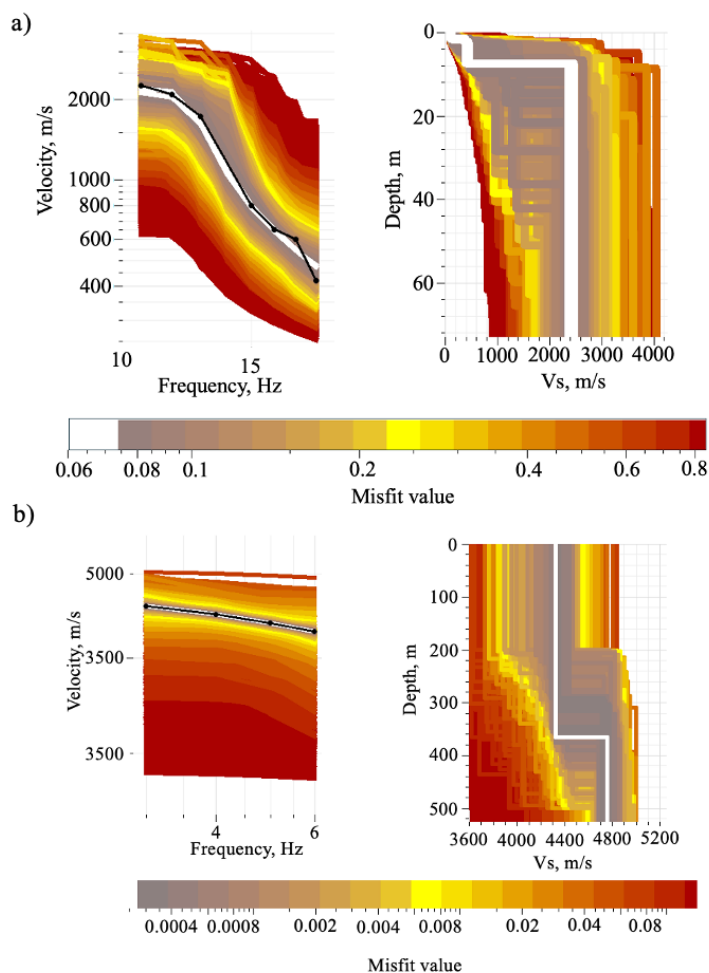
Figure 18: An example of dispersion curves inversion results: a) high frequency (near-surface); b) low frequency (fig.14). The plots demonstrate the ensemble of all velocity models that equally fit the data and prior information. The colour scale indicates the value of the misfit function.

Figure 18 shows for both cases, that the theoretical and empirical dispersion curves were matched with very low misfits: less than 7% for the near-surface model and less than 0.1% for the model of the deeper part, respectively. Finally, we combined all the 1-D calculated velocity models into one 2-D S-wave velocity model below the seismic profile (Figure 19).
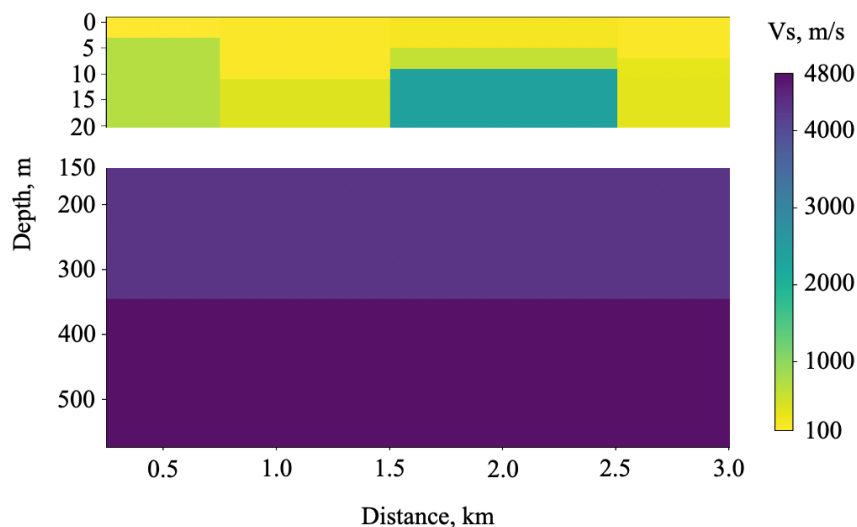
Figure 19: 2D S-wave velocity model of the medium along the profile.

5 Results

Compiled converted arrivals with estimated depths of conversion are shown in Fig. 20 (a, b), in which two major inclined conversion boundaries are seen in RZ and ZR components.

355   The positions of these boundaries are in correlation with the surface geology (Fig. 1a), and they correspond to the two mineralized zones inside the intrusion. The zone with Cr mineralization is traceable to a depth of about 4.5 km, while the zone with V mineralization is traceable to a depth of about 2.6 km. After the offset of 2.5 km along the profile the converted arrivals become invisible, as they are cut with the vertical relatively wide zone showing mainly scattered wavefield. We suggest that it is indication of presence of some near-vertical fault that traps and scatters the incoming wavefield. Several

360   converted arrivals between distances 0.1 and 1 km are visible at times of about 0.3-0.4 s, 0.55-0.6 s and about 0.9 s (marked with red in Fig. 20). They are probably corresponding to converted (and multiple) waves at some sub-horizontal boundary with high acoustic impedance contrast. As there is no drilling data in this part of the profile, it is not possible to correlate these arrivals with lithology.

   The S-wave velocities were obtained with the dispersion curve inversion (Fig. 19) and in the uppermost layer these are

365   between 100 and 400 m/s, which are typical for sedimentary rocks. The second layer is more inhomogeneous and velocities in this layer are varying along the profile from 500-700 m/s on the sides of the profile to 1500-2500 m/s on its central part. This layer may contain fractured volcanic rocks with different cracks densities. The velocities on deeper layers at depths of 150-500 m are about 4300 m/s and 4800 m/s, which are typical for mafic (the top layer) and ultramafic (the deepest layer) volcanic rocks, respectively (Dortman, 1992; Schön, 2015).

370
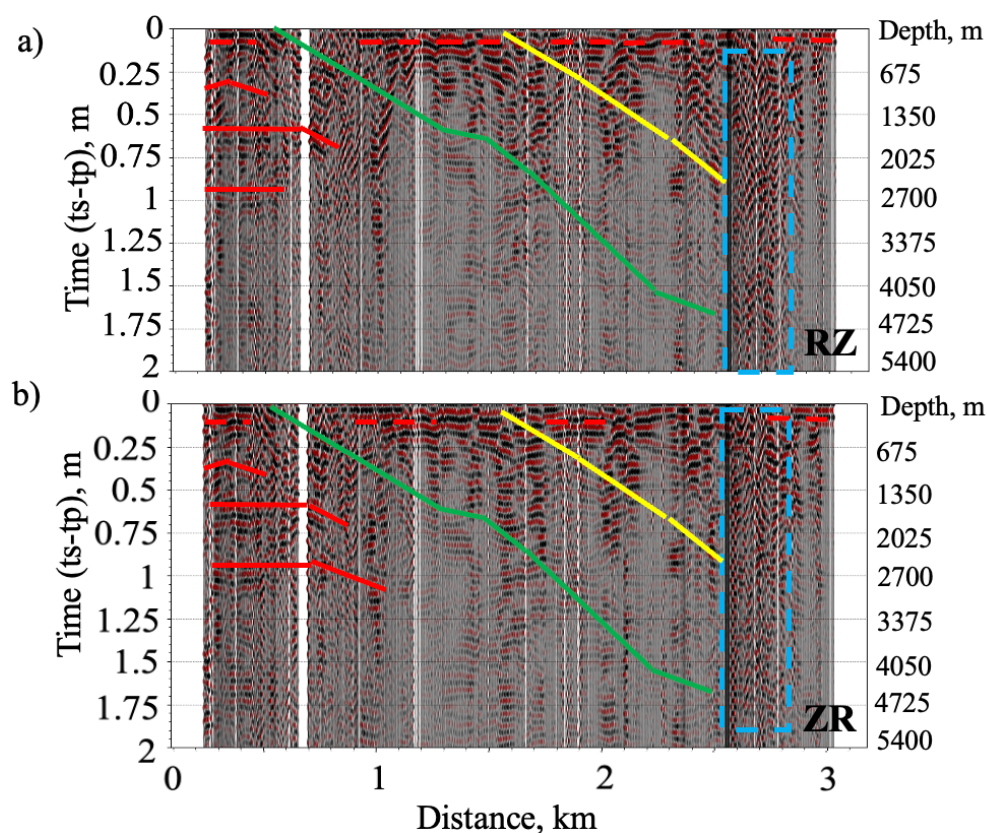
Figure 20: Converted arrivals (green lines – originated on zone with Cr mineralization; yellow lines – originated on zone with V mineralization; red dashed line – converted waves, originated on boundary at the depth of 350 m, presented on figure 18 (boundary between mafic and ultramafic rocks) blue dashed rectangle – fault zone; red lines – converted arrivals originated on unidentified boundaries): a) PS – arrivals; b) SP – arrivals.

Comparison of velocity models (Fig. 18b, Fig. 19) with depths of conversion boundaries (Fig. 20) suggests that converted waves arrived at times of about 0.15 s may originate on the boundary between these layers. The velocities between depths of 20 and 150 m were not estimated because of absence of signals on correspondent frequencies. This can be a signature of the strongly inhomogeneous layer where the signal is scattered and become invisible because of overlapping (interference) between direct and reflected (scattered) waves.

6 Discussion and conclusions

In spite of numerous applications of ground-based near-vertical reflection seismics in exploration and mining planning in hard rock terrains, detection of steeply dipping boundaries associated with mineralisation remains a challenge, even with the 3-D acquisition geometry (Kukkonen et al., 2011; Mahehmir et al. 2012a; Cheradi et al., 2012). However, such boundaries

are routinely detected in VSP measurements with different position of incoming wavefront with respect to target (Bellefleur et al., 2004; Malehmir et al., 2012b). Numerical simulation of wavefield from controlled sources using finite-difference methods predicts that dipping boundaries or ore bodies with contrasting elastic properties produce wavefield that is dominated by shear-wave events and contain converted waves (Bohlen et al., 2003; Bellefleur et al., 2012) that are better detected from 3 component seismic data. However, previous modelling was mainly investigating scattering of the wavefield in massive sulfide deposits. Our numerical modelling was aiming to investigate the scattered wavefield in the orthomagmatic mineral deposits that was not considered in the previous studies. It shows that converted waves produced by a plane-wave source can also be identified in 3-component recordings and utilised for the purpose of detection of steeply dipping boundaries. We showed that converted PS and SP arrivals could be retrieved from body wave part of empirical Green's tensor using cross-correlation of a P-wave coda of regional seismic events recorded along the high-resolution passive seismic profile. Using coda wave passive seismic interferometry with local and regional events, we obtained important information about inner structure of the Akanvaara layered intrusion, namely, detected several conversion boundaries. Two of them correlate on the surface with Cr and V mineralised structures. Converted seismic arrivals, from the V mineralization zone are traceable up to depths of 2.6 km and the ones from Cr mineralization zone are can be followed to depths of about 4.5 km. Moreover, surface wave coda wave interferometry with regional and local events provided information about S-wave velocities in the same seismic profile from ground surface down to 500 m. Obtained velocities agree with petrophysical data. Generally, it could be concluded that regional coda wave passive seismic interferometry is a promising exploration method for orthomagmatic mineral deposits, in which mineralised bodies are often lacking clear electromagnetic response. It can be used as an effective and environmentally friendly tool for greenfield and brownfield exploration of ore deposits.

Author contribution: NA: conceptualization of the research, planning and conducting the passive seismic experiment, software development, data processing, interpretation of the results, the manuscript preparation; EK: conceptualization and supervision of the research, interpretation of the results, the manuscript preparation; KM: planning organizing and conducting passive seismic experiment. Took part in the manuscript preparation; SY: PI of the SEMACRET project. Took part in the interpretation of the results and the manuscript preparation; JS: took part in the numerical simulation and the manuscript preparation.

Competing interests: The authors declare that they have no conflict of interest

Acknowledgements

415   This work is a part of the SEMACRET project: ("Sustainable exploration for orthomagmatic (critical) raw materials in the EU: Charting the road to the green energy transition"). The authors wish to thank CSC - IT Center for Science, Finland (urn: nbn:fi: research-infras-2016072531) and the Open Geospatial Information Infrastructure for Research (Geoportti, urn: nbn:fi: research-infras-2016072513) for computational resources and support.

References

420   Afonin, N., Kozlovskaya, E., Nevalainen, J., and Narkilahti, J.: Improving the quality of empirical Green's functions, obtained by cross-correlation of high-frequency ambient seismic noise, Solid Earth, 10(5), 1621-1634, 2019.

Afonin, N., Kozlovskaya, E., Heinonen, S., and Buske, S.: Near-surface structure of the Sodankylä area in Finland, obtained by passive seismic interferometry, Solid Earth, 12, 1563–1579, https://doi.org/10.5194/se-12-1563-2021, 2021.

Afonin, N: Development of passive seismic interferometry to study shallow subsurface structure. PhD thesis, 2022

425   Aki, K., and Richards, P.G.: Quantitative Seismology. 2nd Edition, CA: Univ. Sci. Books, Sausalito, 700, 2002.

Alapieti, T.T., Filen, B.A., Lahtinen, J.J., Lavrov, M.M., Smolkin, V.F. and Voitsekhovsky, S.N.: Early Proterozoic layered intrusions in the northeastern part of the Fennoscandian Shield, 1990.

Bellefleur, G., Müller, C., Snyder, D., and Matthews, L.: Downhole seismic imaging of a massive sulfide orebody with mode-converted waves, Halfmile lake, New Brunswick, Canada, GEOPHYSICS 69: 318-329, 2004.

430   Bellefleur, G., Malehmir, A., Müller, C.: Elastic finite-difference modeling of volcanic-hosted massive sulfide deposits: A case study from Half Mile Lake, New Brunswick, Canada, GEOPHYSICS 77: WC25-WC36, 2012.

Bensen, G. D., Ritzwoller, M. H., Barmin, M. P., Levshin, A. L., Lin, F., Moschetti, M. P., ... and Yang, Y.: Processing seismic ambient noise data to obtain reliable broad-band surface wave dispersion measurements. Geophysical journal international, 169(3), 1239-1260, 2007.

435   Bohlen, T.: Parallel 3-D viscoelastic finite difference seismic modelling. Computers & Geosciences, 28(8), 887-899, 2002.

Bohlen,T., Miller, C. and Milkereit, B.: Elastic Seismic Wave Scattering from Massive Sulfde Orebodies: On the Role of Composition and Shape. In: Eaton, D. W., Milkereit, B. and Salisbury, M H. (eds) Hardrock Seismic Exploration. Geophysicsl Development Series, SEG, https://doi.org/10.1190/1.9781560802396, 2003.

Bostock, M. G.: Green's functions, source signatures, and the normalization of teleseismic wave fields, J. Geophys. Res.,

440   109, B03303, doi:10.1029/2003JB002783, 2004.

Cheraghi, S., Malehmir, A., and Bellefleur, G.: 3D imaging challenges in steeply dipping mining structures: New lights on acquisition geometry and processing from the Brunswick no. 6 seismic data, Canada, GEOPHYSICS 77: WC109-WC122. https://doi.org/10.1190/geo2011-0475.1., 2012.

Claerbout, J. F.: Synthesis of a layered medium from its acoustic transmission response. Geophysics, 33(2), 264-269, 1968.

445   Dortman, N. B.: Handbook Petrophysics, Nedra, Moscow, 390 pp, 1992.

European Commission: European Critical Raw Materials Act: https://ec.europa.eu/commission/presscorner/detail/en/ip_23_1661. Accessed 12.04.2024 , 2023(a).

Greenhalgh, S. A., Zhou, B., and Cao, S.: A crosswell seismic experiment for nickel sulphide mineralization: Journal of Applied Geophysics, 53, 77–89, 2003.

450   Hanski, E., Walker, R., Huhma, H., and Suominen, I.: The Os and Nd isotopic systematics of c. 2.44 Ga Akanvaara and Koitelainen mafic layered intrusions in northern Finland. Precambrian Research,109, 73-102. 10.1016/S0301-9268(01)00142-5, 2001.

Janik, T., Kozlovskaya, E., Heikkinen, P., Yliniemi, J., and Silvennoinen, H.: Evidence for preservation of crustal root beneath the Proterozoic Lapland-Kola orogen (northern Fennoscandian shield) derived from P and S wave velocity models

455   of POLAR and HUKKA wide-angle reflection and refraction profiles and FIRE4 reflection transect. Journal of Geophysical Research: Solid Earth, 114(B6), 2009.

Koistinen, T., Stephens, M. B., Bogatchev, V., Nordgulen, Ø., Wennerström, M., and Korhonen, J.: Geological map of the Fennoscandian Shield, scale 1: 2,000,000: Geol. Surv. Finland, Norway and Sweden and the North-West Dept. of Nat. Res. of Russia, 2001.

460   Konnunaho, J.P., Hanski, E.J., Bekker, A., Halkoaho, T.A.A., Hiebert, R.S. and Wing, B.A.: The Archean komatiite-hosted, PGE-bearing Ni–Cu sulfide deposit at Vaara, eastern Finland: evidence for assimilation of external sulfur and post-depositional desulfurization. Mineralium Deposita, 48, pp.967-989, 2013.

Kukkonen, I., Heikkinen, P., Heinonen, S. E., Laitinen, J., and HIRE Working Group of the Geological Survey of Finland: Reflection seismics in exploration for mineral deposits: initial results from the HIRE project. In K. Nenonen, and P. Nurmi

465   (Eds.), Geoscience for Society: 125th Anniversary Volume (Special Paper 49). Geological Survey of Finland, 2011.

Lauri, L. S., Rämö, O. T., Huhma, H., Mänttäri, I., and Räsänen, J.: Petrogenesis of silicic magmatism related to the~ 2.44 Ga rifting of Archean crust in Koillismaa, eastern Finland. Lithos, 86(1-2), 137-166, 2006.

Lutynski, P: Akanvaara project, Finland: Technical report, Strategic Resources Inc., 49 pp., 2019.

Maier, W.D. and Hanski, E.J.: Layered Mafic–Ultramafic Intrusions of Fennoscandia: Europe's Treasure Chest of Magmatic

470   Metal Deposits. Elements: An International Magazine of Mineralogy, Geochemistry, and Petrology, 13(6), pp.415-420, 2017.

Malehmir, A., Urosevic, M., Bellefleur, G., Juhlin, C., and Milkereit, B.: Seismic methods in mineral exploration and mine planning — Introduction, GEOPHYSICS 77: WC1-WC, https://doi.org/10.1190/2012-0724-SPSEIN.1, 2012a.

Malehmir, A., Juhlin, C., Wijns, C., Urosevic, M., Valasti, P., and Koivisto, E.: 3D reflection seismic imaging for open-pit

475   mine planning and deep exploration in the Kevitsa Ni-Cu-PGE deposit, northern Finland, GEOPHYSICS 77: WC95-WC108.https://doi.org/10.1190/geo2011-0468.1, 2012b.

Moilanen, M., Hanski, E., Konnunaho, J., Yang, S.H., Törmänen, T., Li, C. and Zhou, L.M.: Re-Os isotope geochemistry of komatiite-hosted Ni-Cu-PGE deposits in Finland. Ore Geology Reviews, 105, pp.102-122, 2019.

Mutanen, T.: Geology and ore petrology of the Akanvaara and Koitelainen mafic layered intrusions and the Keivitsa-

480   Satovaara layered complex, northern Finland, Geological Survey of Finland, Bulletin 395, 240 pages, 1997.

Mutanen, T.: Akanvaaran Intruusion Kromi-, Kromi-Vanadiini-, Vanadiini-Ja Platinametalli-Kultaesiintymät, Geologian Tutkimuskeskus, 107 pages (in Finnish), 1998.

Mutanen, T.: Field Trip Guidebook: The Akanvaara Intrusion and the Keivitsa-Satovaara Complex, with stops at

Park, C. B., Miller, R. D., and Xia, J.: Multichannel analysis of surface waves. Geophysics, 64(3), 800-808, 1999.

485   Schön, J. H.: Physical properties of rocks: Fundamentals and principles of petrophysics. Elsevier, 2015.

Shuster, G.T.: Seismic interferometry: Cambridge University press, 2009.

Pripachkin, P.V., Neradovsky, Y.N., Fedotov, Z.A., Nerovich, L.I., Voytekhovsky, Y.L., Chistjakova, L.D., Mansurova, N.A.: The Cu-Ni-PGE and Cr deposits of the Monchegorsk area, Kola Penisula, Russia. In: Hanski EJ, Maier WD (eds) Ni-Cr-PGE Deposits of Finland and the Kola Peninsula. Excursion Guidebook, 12th Biennial SGA Meeting, Uppsala, Sweden,

490   90 pp, 2013.

Snieder, R.: The theory of coda wave interferometry, Pure and Applied geophysics, 163, 455-473, 2006.

Tiira, T., Janik, T., Kozlovskaya, E., Grad, M., Korja, A., Komminaho, K., Hegedus, E., Kovacs, C. A., Silvennoinen, H. and Bruckl, E.: Crustal Architecture of the Inverted Central Lapland Rift Along the HUKKA 2007 Profile. Pure and Applied geophysics, 171, 7, 1129-1152. https://doi.org/10.1007/s00024-013-0725-3, 2014.

495   Vinnik, L. P.: Detection of waves converted from P to SV in the mantle, Physics of the Earth and planetary interiors, 15(1), 39-45, 1977.

Wang, C., Tauzin, B., Pham, T.-S., and Tkalčić, H.: On the efficiency of P-wave coda autocorrelation in recovering crustal structure: Examples from dense arrays in the eastern United States. Journal of Geophysical Research: Solid Earth, 125, e2020JB020270. https://doi.org/10.1029/2020JB020270, 2020.

500   Zhu, L., and Kanamori, H.: Moho depth variation in southern California from teleseismic receiver functions. Journal of Geophysical Research: Solid Earth, 105(B2), 2969-2980, 2000.